JPET Fast Forward. Published on December 10, 2020 as DOI: 10.1124/jpet.120.000086
This article has not been copyedited and formatted. The final version may differ from this version.

ORIGINAL ARTICLE SUBMISSION

TITLE PAGE

Title:

Distinct uptake kinetics of Alzheimer's disease amyloid beta 40 and 42 at the blood-brain barrier endothelium

Author names and affiliation:

Nidhi Sharda, Kristen M. Ahlschwede, Geoffry L. Curran, Val J. Lowe and Karunya K. Kandimalla

N.S. and K.K.K.: Department of Pharmaceutics and the Brain Barriers Research Center, College of Pharmacy, University of Minnesota, Minneapolis, MN, USA

K.M.A.: Department of Pharmaceutical Sciences, Rosalind Franklin University of Medicine and Science, College of Pharmacy, North Chicago, IL, USA

G.L.C. and V.J.L.: Department of Radiology, Mayo Clinic College of Medicine, Rochester, MN, USA

G.L.C and K.K.K.: Department of Neurology, Mayo Clinic College of Medicine, Rochester, MN, USA

Note: N.S.: Current affiliation: Department of Clinical Pharmacology & Pharmacometrics, Bristol-Myers Squibb, Princeton, NJ, USA

Primary Laboratory of origin

Kandimalla Laboratory

9-149 Weaver Densford Hall

JPET Fast Forward. Published on December 10, 2020 as DOI: 10.1124/jpet.120.000086
This article has not been copyedited and formatted. The final version may differ from this version.

Department of Pharmaceutics and the Brain Barriers Research Center, College of Pharmacy, University of Minnesota, Minneapolis, MN 55455, USA

JPET Fast Forward. Published on December 10, 2020 as DOI: 10.1124/jpet.120.000086
This article has not been copyedited and formatted. The final version may differ from this version.

RUNNING TITLE PAGE

Running Title:

Amyloid beta 40/42 uptake kinetics at the BBB

Corresponding author:

Karunya K. Kandimalla,

Department of Pharmaceutics and the Brain Barriers Research Center, College of Pharmacy,

9-149A Weaver-Densford Hall, 308 Harvard Street SE,

University of Minnesota, Minneapolis, MN 55455, USA

Email: kkandima@umn.edu

Number of text pages:37

Number of tables: 3

Number of figures: 3 + 1 (supplementary section)

Number of references: 54

Number of words in Abstract: 250

Number of words in Introduction: 494

Number of words in Discussion: 1589

Non-standard abbreviation list (alphabetical order)

JPET Fast Forward. Published on December 10, 2020 as DOI: 10.1124/jpet.120.000086
This article has not been copyedited and formatted. The final version may differ from this version.

Alzheimer's disease (AD), Amyloid beta 40 (Aβ40), Amyloid beta 42 (Aβ42), Blood-brain barrier (BBB), Human brain microvascular endothelial (hCMEC/D3), Single photon emission computed tomography/computed tomography (SPECT/CT),

Recommended section: Metabolism, Transport, and Pharmacogenomics

JPET Fast Forward. Published on December 10, 2020 as DOI: 10.1124/jpet.120.000086
This article has not been copyedited and formatted. The final version may differ from this version.

ABSTRACT:

Blood-brain barrier (BBB) endothelial cell lining the cerebral microvasculature maintain dynamic equilibrium between soluble amyloid beta (Aβ) levels in the brain and plasma. The BBB dysfunction prevalent in Alzheimer's disease contributes to the dysregulation of plasma and brain Aβ and leads to the perturbation of ratio between Aβ42 and Aβ40, two most prevalent Aβ isoforms in Alzheimer's patients. We hypothesize that BBB endothelium distinguishes between Aβ40 and Aβ42, distinctly modulates their trafficking kinetics between plasma and brain and thereby contributes to the maintenance of healthy Aβ42/Aβ40 ratios. To test this hypothesis, we investigated Aβ40 and Aβ42 trafficking kinetics in hCMEC/D3 monolayers (human BBB cell-culture model) *in vitro* as well as in mice *in vivo.* While the rates of uptake of fluorescein labeled Aβ40 and Aβ42 (F-Aβ40 and F-Aβ42) were not significantly different on the abluminal side, the luminal uptake rate of F-Aβ42 was substantially higher than F-Aβ40. Since, higher plasma Aβ levels were shown to aggravate BBB dysfunction and trigger cerebrovascular disease, we systematically investigated the dynamic interactions of luminal ^{125}I-Aβ peptides and their trafficking kinetics at BBB using single-photon-emission-computed-tomography/computed-tomography (SPECT/CT) imaging in mice. Quantitative modeling of the dynamic imaging data thus obtained showed that the rate of uptake of toxic ^{125}I-Aβ42 and its subsequent BBB transcytosis is significantly higher than ^{125}I-Aβ40. It is likely that the molecular mechanisms underlying these kinetic differences are differentially affected in Alzheimer's and cerebrovascular diseases, impact plasma and brain levels of Aβ40 and Aβ42, engender shifts in Aβ42/Aβ40 ratio, and unleash downstream toxic effects.

JPET Fast Forward. Published on December 10, 2020 as DOI: 10.1124/jpet.120.000086
This article has not been copyedited and formatted. The final version may differ from this version.

Significance Statement:

Dissecting the binding and uptake kinetics of Aβ40 and Aβ42 at the BBB endothelium will facilitate the estimation Aβ40 versus Aβ42 exposure to the BBB endothelium and allow us to assess the risk of BBB dysfunction by monitoring Aβ42 and Aβ40 levels in the plasma. This knowledge, in turn, will aid in elucidating the role of these predominant Aβ isoforms in aggravating BBB dysfunction and cerebrovascular disease.

JPET Fast Forward. Published on December 10, 2020 as DOI: 10.1124/jpet.120.000086
This article has not been copyedited and formatted. The final version may differ from this version.

INTRODUCTION

Alzheimer's disease research thus far has been predominantly neurocentric with limited effort focused on investigating the influence of systemic and non-neuronal systems on the disease progression. Specifically, pathophysiological mechanisms driving the neurovascular unit (NVU) dysfunction is one of the underexplored areas. The vascular components of the NVU, constituting of the blood-brain barrier (BBB) endothelium and pericytes, interface with neurons and astrocytes in the brain parenchyma (Bell *et al*, 2007; Deane *et al*, 2009). These vascular and neuronal components are seamlessly integrated into a cohesive unit such that disruption to one component influences the integrity and function of the other (Zlokovic, 2010; Erickson and Banks, 2013).

The two-hit hypothesis of Alzheimer's disease (AD) proposed by Zlokovic (Zlokovic, 2011) emphasized this interconnectivity and posited that the pathological manifestations in Alzheimer's brain are secondary and subsequent to the primary insult sustained by the BBB endothelium. Vascular risk factors, such as metabolic syndrome and inflammatory changes in the periphery, may constitute the first hit and result in BBB dysfunction. Since the BBB endothelium plays a central role in maintaining dynamic equilibrium between plasma and brain Aβ levels (Bowman and Quinn, 2008; Deane *et al*, 2009), the BBB dysfunction could affect Aβ levels in plasma and brain and alter Aβ42/Aβ40 ratios (Marques *et al.*, 2009). These changes are thought to render the second hit by triggering neuropathological symptoms in the brain and accelerating cognitive decline (Toledo *et al.*, 2013; Fandos *et al.*, 2017).

Another important, yet under investigated dimension of this hypothesis is the role of plasma Aβ in exacerbating neurocognitive changes. Literature reports indicate that increase in plasma Aβ levels and shifts in Aβ42/Aβ40 ratios intensify BBB dysfunction, propel the positive

feedback loop, and accelerate neurodegenerative changes (DeMattos *et al.*, 2001; Marchi *et al.*, 2004; Ascolani *et al.*, 2012; Erickson and Banks, 2013; Eisele *et al.*, 2014; Koizumi *et al.*, 2016; Poljak and Sachdev, 2017; Govindpani *et al.*, 2019). Recently, Aβ40 and Aβ42 were suggested to have distinct effects on this positive feedback loop. Higher Aβ40 concentration in plasma was shown to be associated with an elevated risk of dementia compared to Aβ42 (van Oijen *et al.*, 2006). On the other hand, Aβ42 in the brain was shown to trigger substantially greater neurodegeneration (Younkin, 1998; Cleary *et al.*, 2005) and tau hyperphosphorylation (Lacor *et al.*, 2007; Ryan *et al.*, 2009; Hu *et al.*, 2014) than Aβ40. However, differing by only two amino acids and being recognized by the same receptors on the luminal side [receptor for advance glycated end products (RAGE)] and on the abluminal side [low density lipoprotein receptor-related protein 1 (LRP1)], it is unclear how Aβ40 and Aβ42 could manifest these differential effects.

We addressed this question by investigating the kinetics of Aβ40 and Aβ42 interactions and their subsequent uptake at the BBB endothelium. This knowledge is expected to help determine the extent of Aβ40 versus Aβ42 exposure to the BBB endothelium, assess the risk of BBB dysfunction, and associate it with the downstream neuropathological changes.

JPET Fast Forward. Published on December 10, 2020 as DOI: 10.1124/jpet.120.000086
This article has not been copyedited and formatted. The final version may differ from this version.

MATERIALS AND METHODS

***Reagents and Lab supplies*:** ^{125}I was obtained from Perkin-Elmer Life and Analytical Sciences (Boston, MA). Plasticware was obtained from Corning Life Sciences (Tewksbury, MA), USA Scientific (Ocala, FL) or Denville Scientific Inc. (South Plainfield, NJ).

***Synthesis of native, fluorescein labeled and radioiodinated Aβ peptides*:** Aβ40, fluorescein labeled Aβ40 (F-Aβ40), Aβ42, and F-Aβ42 were synthesized as described earlier (Kandimalla *et al.*, 2005; Omtri *et al.*, 2012; Agyare *et al.*, 2013; Swaminathan *et al.*, 2018) and Aβ monomers were prepared according to the procedure described by Klein (Klein *et al.*, 2004). Briefly, Aβ peptides were accurately weighed, dissolved in ice cold 1,1,1,3,3,3 hexafluoroisopropanol (HFIP) (MP Biomedicals, Santa Ana, CA), and incubated at room temperature for 60 min. The resultant solutions were chilled on ice, aliquoted appropriately, and allowed to dry overnight. The HFIP traces were further removed by vacuum evaporation, and the dried films were stored at -20 °C. Before each experiment, the Aβ films were dissolved in anhydrous dimethyl sulfoxide (DMSO), diluted in Ham's F-12 medium (Mediatech, Manassas, VA), and centrifuged at 18,000 rpm to remove any insoluble Aβ aggregates. Radioiodination of Aβ40 and Aβ42 was conducted using the chloramine-T procedure as described in our previous publications (Poduslo *et al.*, 1997; Kandimalla *et al.*, 2005). Free radioactive iodine was removed by dialysis against 0.01 M phosphate-buffered saline (PBS) at pH 7.4 (Sigma-Aldrich, St. Louis, MO). The extent of radiolabeling of Aβ peptides was determined by trichloroacetic acid (TCA) precipitation. The radioiodinated Aβ preparations were used in the experiments only if the TCA precipitable counts were greater than 95 % of the total counts. The specific activity of ^{125}I-Aβ40 and 42 was determined to be in the range of 45-48 μCi/μg.

JPET Fast Forward. Published on December 10, 2020 as DOI: 10.1124/jpet.120.000086
This article has not been copyedited and formatted. The final version may differ from this version.

***Cell culture*:** All cell culture experiments were performed on transformed cell lines in BCL-2 hood as required by the Institutional Biological Safety Committee at the University of Minnesota, MN. Human brain microvascular endothelial (hCMEC/D3) cells were a gift from Dr. Pierre-Oliver Couraud (INSERM U1016, Institut Cochin, Paris, France). The hCMEC/D3 cells were grown in endothelial cell growth basal (EBM-2) medium (Lonza, NJ) supplemented with 1 ng/mL human basic fibroblast growth factor (PeproTech, NJ), 10 mM HEPES, 1 % chemically defined lipid concentrate (Gibco, NY), 5 µg/mL ascorbic acid, 1.4 µM hydrocortisone, 1 % penicillin-streptomycin (MP Biomaterials, OH) and 5 % of fetal bovine serum (FBS). Polarized hCMEC/D3 cell monolayers were cultured on collagen (Corning, MA) coated 6 well plates or Transwell® filters (Corning Costar™, MA) under 5 % CO_2 at 37 °C. Trans-endothelial electrical resistance (TEER), representative of tight junctional integrity of the monolayers, was measured using chopstick electrodes attached to EVOM meter (World Precision Instruments, Sarasota, FL). The TEER values of hCMEC/D3 monolayers were found to be around 70-80 Ω cm^2.

Flow cytometry: Following the treatment with F-Aβ, hCMEC/D3 cell monolayers were washed thoroughly with PBS, gently trypsinized with trypsin-EDTA for 30 sec and neutralized with FBS. The dislodged cells were washed twice using ice cold PBS, fixed with 4 % paraformaldehyde (PFA) solution and the intracellular fluorescence was quantified using BD FACSCalibur™ flow cytometer. The F-Aβ40 and F-Aβ42 intracellular fluorescence intensities were measured using 488 nm laser fitted with 530/30 filter. Data was acquired with BD CellQuest™ Pro and analyzed using FlowJo software. Intracellular fluorescence units (IFU) are presented as geometric means ± geometric standard deviation.

JPET Fast Forward. Published on December 10, 2020 as DOI: 10.1124/jpet.120.000086
This article has not been copyedited and formatted. The final version may differ from this version.

Kinetics of F-Aβ40 or F-Aβ42 uptake at BBB endothelium in vitro

F-Aβ uptake kinetics as a function of concentration: Polarized hCMEC/D3 cell monolayers were incubated with increasing concentrations of F-Aβ40 or F-Aβ42 (0.06 μM to 0.9 μM) for 30 min at 37 °C or 4 °C. The cells were harvested and analyzed using flow cytometry as described. The observed intracellular fluorescence (geometric mean ± geometric SD) was plotted as a function of F-Aβ concentration (μM).

F-Aβ uptake kinetics as a function of time: Polarized hCMEC/D3 monolayers grown on Transwell® filters were incubated with 0.45 μM of F-Aβ40 or F-Aβ42 on either luminal (L) or abluminal (A) side for various lengths of time (15-60 min) and the intracellular uptake was assessed by flow cytometry. The observed geometric mean was plotted as a function of time, and rate of uptake was estimated by fitting the data to linear regression model using GraphPad Prism® software.

Kinetics of Aβ40 and Aβ42 uptake at the BBB endothelium in vivo

Animals: The B6SJLF1 mice, which will be hereafter referred to as wild-type mice (WT), were procured from Jackson Laboratory (Bar Harbor, ME). The mice were housed in virus-free barrier facility with 12-hour light and dark cycle and were provided with pellet food and purified water ad libitum. Male and female mice between ages of five and eight months were randomly distributed among various groups (n=3 each for plasma PK and brain SPECT/CT, respectively, for Aβ40 and Aβ42). All animal studies were conducted in a single blinded fashion and only the details required for conducting the studies were provided to the experimenters. All animal experiments were conducted as per the National Institutes of Health guidelines for the care and

JPET Fast Forward. Published on December 10, 2020 as DOI: 10.1124/jpet.120.000086
This article has not been copyedited and formatted. The final version may differ from this version.

use of laboratory animals, and protocols approved by the Mayo Clinic Institutional Animal Care and Use Committee, Rochester, MN. Data in this manuscript are reported according to the ARRIVE guidelines.

Plasma pharmacokinetic (PK) studies using Gamma counter: WT mice were anesthetized using a mixture of isofluorane and oxygen (1.5 % and 4 L/min). Femoral vein and femoral artery were catheterized under general anesthesia. Single IV bolus dose of ^{125}I-Aβ40 or ^{125}I-Aβ42 equivalent to 100 μCi/100μL was administered through the femoral vein. The blood was sampled (20 μL) from the femoral artery at various time points of 0.25, 1, 3, 5, 10 and 15 min. The recovered plasma was subjected to tricholoacetic acid (TCA) precipitation and the ^{125}I radioactivity in the precipitate and supernatant was assayed using gamma counter (Cobra II; PerkinElmer Life and Analytical Sciences, Boston, MA). The radioactivity in the precipitate was deemed to be associated with the intact protein.

Brain uptake studies using dynamic Single Photon Emission Computed Tomography coupled with computed tomography (SPECT/CT): A 500 μCi dose of ^{125}I-Aβ40 and ^{125}I-Aβ42 in 100 μL was administered to WT mice via femoral vein. Brain uptake of ^{125}I-Aβ radioactivity was determined by dynamic planar imaging (Gamma Medica-Ideas Pre-Clinical Imaging, Northridge, CA) using a low energy and high resolution parallel-hole collimator with 12.5 cm FOV and 13:36 min acquisition time. Over 64 projections (10 sec per projection) were obtained with a reported resolution 1 to 2 μm. Then CT scans were acquired on a continuous circular orbit with a 50 μm slice thickness. A total of 256 images at 80 kVp and 0.28 mA current were acquired at a reported resolution of 43 μm. Dynamic SPECT and CT images were processed and analyzed

JPET Fast Forward. Published on December 10, 2020 as DOI: 10.1124/jpet.120.000086
This article has not been copyedited and formatted. The final version may differ from this version.

using Biomedical Image Quantification and Kinetic Modeling Software version 2.85 (PMOD Technologies, Switzerland).

Evaluation of Aβ interactions with the BBB and subsequent brain uptake by Logan and Patlak plots. Logan and Patlak approaches describe ways to linearize the blood-to-brain distribution of ^{125}I-Aβ, without making any assumptions on the particular arrangement or the number of compartments involved. While the Logan plot describes reversible kinetics with a slope parameter attributed to the distribution volume (V_T) (Logan *et al.*, 1990), the Patlak plot describes irreversible kinetics predicting the influx clearance (K_i) (Patlak *et al*., 1983). The initial interactions between plasma and the BBB endothelium, described by dynamic SPECT/CT data, during the first 5 min following IV bolus injection were assumed to reflect the reversible kinetics at the surface of the BBB and the subsequent transfer beyond 5 min was assumed to reflect irreversible uptake into brain parenchyma (> 5 min). Therefore, first five minutes (0-5 minutes) SPECT/CT data was used to construct the Logan plot and the 5-40 minutes data was used to construct the Patlak plot. Plasma observations were simulated for individual animals with the plasma PK parameters predicted using experimental data.

The Logan equation for reversible kinetics is:

$$\frac{\int_0^t A_{brain}dt}{A_{brain\,(t)}} = V_T . \frac{\int_0^t C_p dt}{A_{brain\,(t)}} + \mathrm{b}$$

(1)

where, $A_{brain\,(t)}$ is the amount of ^{125}I-Aβ radioactivity associated with the brain as measured by SPECT/CT (μCi) at time t; $\int_0^t A_{brain}dt$ is the area under the brain radioactivity-time curve from time '0' to 't' (μCi. min); $C_{p(t)}$is the plasma ^{125}I-Aβ concentration at t (μCi/mL); $\int_0^t C_p dt$ is the

JPET Fast Forward. Published on December 10, 2020 as DOI: 10.1124/jpet.120.000086
This article has not been copyedited and formatted. The final version may differ from this version.

area under the plasma concentration-time curve from time '0' to 't' (μCi/mL.min); V_T is the slope of the linear equation referred to as the distribution volume (mL); and b is the intercept of the linear equation (min). The Logan plot was generated by plotting $\frac{\int_0^t A_{brain} dt}{A_{brain\,(t)}}$ as a function of $\frac{\int_0^t C_p dt}{A_{brain\,(t)}}$

To assess the influx of ^{125}I-Aβ40 or ^{125}I-Aβ42 from plasma into the brain, Patlak plot was constructed by the following equation:

$$\frac{A_{brain\,(t)}}{C_{p(t)}} = K_i \frac{\int_0^t C_p dt}{C_{p(t)}} + V_0 \quad (2)$$

where, K_i, the influx clearance into the brain (mL/min) was determined as the slope parameter. V_0, is the intercept of the linear equation referring to the volume of the vascular compartment (mL).

Thus, the Logan plot is linear when transient equilibrium between the plasma and BBB endothelium is attained (lag time), and remains linear until the ligand is associated with BBB endothelium and displays reversible kinetics. This linearity is lost when the ligand entered brain compartment, irreversibly.

Resolution of Aβ interactions with the BBB by PK compartmental modeling. A three-compartment model comprising of plasma and highly perfused tissues; other peripheral organs and tissues; and BBB endothelium as well as the brain parenchyma, was constructed. Forward and reverse rate constants describing the transfer between plasma and tissue are k_{12} and k_{21} respectively, whereas the transfer rate constants between plasma and BBB endothelium are designated as k_{13} and k_{31}. The elimination rate constant from the plasma compartment was k_{10}.

JPET Fast Forward. Published on December 10, 2020 as DOI: 10.1124/jpet.120.000086
This article has not been copyedited and formatted. The final version may differ from this version.

It was assumed that the short time exposure to the BBB endothelium (< 5 min) was insufficient to produce detectable levels within the BBB endothelium and the brain compartment; hence, elimination from the brain, which includes enzymatic degradation and brain clearance, was assumed to be negligible. This assumption is valid as the macromolecule such as Aβ is expected to traffic the overall thickness of BBB endothelium, around 2-3 μm (Li *et al.*, 2010), via receptor-mediated endocytosis, which is expected to take well over 15 min. For example, it takes about 30 min for 68 % of transferrin to reach from luminal to the abluminal side of the BBB, whereas, in 5 min only a modest amount of 10-12 % was claimed to reach the abluminal side (Khan *et al.*, 2018). Further, it is known that Logan plot remains linear only until the kinetics are reversible. While the first 5 min signifies the reversible interactions of Aβ peptide with its receptor on the luminal surface of the BBB, the Aβ peptide enters into the irreversible cellular compartment beyond 5 min, and later into the brain parenchyma. This is coincided with the loss of linearity in the Logan plot beyond 5 min as the assumption of reversible uptake is no longer valid (supplementary Figure 1). Based on these observations, 0-5 min data was used for the Logan plot (reversible kinetics at BBB endothelium), whereas 5-40 min data (irreversible kinetics into the cellular compartments and brain parenchyma) was used to construct the Patlak plot. Additionally, uniform mixing is assumed in all compartments and elimination from BBB and the tissue compartment was assumed to be negligible when compared to the elimination from the central compartment.

The initial estimates were obtained for both Aβ40 and Aβ42 based on the *in vitro* uptake studies (k_{13} and k_{31}) and the PK parameters ($k_{12}, k_{21}, k_{10}, V$) predicted by fitting the model described by the following differential equations to *in vivo* plasma and brain data. Initial conditions were $C_{plasma} = \frac{Dose}{V}$ and $C_{tissue} = C_{BBB} = 0$; where, *Dose* refers to the total dose

JPET Fast Forward. Published on December 10, 2020 as DOI: 10.1124/jpet.120.000086
This article has not been copyedited and formatted. The final version may differ from this version.

administered in radioactivity units (µCi), V stands for apparent volume of distribution in milliliters (mL), C_{plasma}, C_{tissue} *and* C_{BBB} represent the concentrations in plasma, tissue and blood brain barrier, respectively.

$$\frac{dC_{plasma}}{dt} = -(k_{10} + k_{13} + k_{12}).C_{plasma} + k_{21}.C_{tissue} + k_{31}.C_{BBB} \quad (3)$$

$$\frac{dC_{tissue}}{dt} = k_{12}.C_{plasma} - k_{21}.C_{tissue} \quad (4)$$

$$\frac{dC_{BBB}}{dt} = k_{13}.C_{plasma} - k_{31}.C_{BBB} \quad (5)$$

Various kinetic parameters were predicted by simultaneously fitting the model to plasma and brain radioactivity obtained by gamma counter and SPECT/CT imaging, respectively and the goodness-of-fit was assessed.

Statistical analyses:

The observed data is expressed as mean ± standard deviation, whereas predicted parameters are presented either as parameter estimate ± standard error or parameter estimate (percent coefficient of variance). Statistical significance (*p<0.05, **p<0.01 and ***p<0.001) of the differences between Aβ40 and Aβ42 kinetics was ascertained by Student's t-test conducted using Prism version 5 (Graph pad software, La Jolla, CA).

JPET Fast Forward. Published on December 10, 2020 as DOI: 10.1124/jpet.120.000086
This article has not been copyedited and formatted. The final version may differ from this version.

RESULTS

We investigated the kinetics of Aβ40 and Aβ42 uptake and transcytosis at the BBB *in vitro* in hCMEC/D3 cell monolayers. The *in vitro* findings were then verified in mice *in vivo* by employing dynamic imaging methods coupled with quantitative modeling techniques.

Distinct uptake kinetics of F-Aβ40 and F-Aβ42 at the BBB endothelium in vitro (Fig. 1, Table I). F-Aβ peptides demonstrated saturable uptake by polarized hCMEC/D3 cell monolayers grown on 6-well plates at 37 °C. However, F-Aβ uptake at 4 °C, when energy dependent endocytic mechanisms were inhibited, was linearly dependent on the donor concentration **(Fig. 1 B)**. In addition, both F-Aβ40 and F-Aβ42 accumulated linearly over time in hCMEC/D3 cell monolayers grown on Transwell® filters, and their cellular accumulation was higher following luminal exposure **(Fig. 1 D)** than upon abluminal exposure **(Fig. 1 E)**. Importantly, slopes of F-Aβ40 or F-Aβ42 uptake by hCMEC/D3 cell monolayers versus time were not significantly different upon abluminal exposure **(Table I)**. However, upon luminal exposure, the slope of F-Aβ42 (1.79 ± 0.12 IFU/min) was found to be significantly (Student's t-test, p***<0.001) greater than that of F-Aβ40 (0.55 ± 0.04 IFU/min).

Determination of ^{125}I-Aβ kinetics at the BBB and brain in vivo using graphical model analyses (Fig. 2, Table II). Dynamic imaging methods allow us to temporally separate ^{125}I-Aβ interactions with the BBB and analyze those using Logan and Patlak plots. The Logan plot describes the reversible interaction of ^{125}I-Aβ with the BBB endothelium, which is assumed to occur within the first five minutes of IV bolus administration. Beyond five minutes, irreversible entry of ^{125}I-Aβ into the BBB endothelium and brain parenchyma predominates and the

JPET Fast Forward. Published on December 10, 2020 as DOI: 10.1124/jpet.120.000086
This article has not been copyedited and formatted. The final version may differ from this version.

corresponding kinetics could be described by the Patlak plot. The Logan plot analysis demonstrated distinct reversible kinetics of ^{125}I-Aβ40 and ^{125}I-Aβ42 and predicted significantly (***p<0.001) higher V_T for ^{125}I-Aβ42 (55.8 ± 1.2 µL) than for ^{25}I-Aβ40 (39.7 ± 0.07 µL) (**Fig. 2 B, Table II)**. Beyond 5 min, linearity of the Logan plots was lost, which may represent switch from reversible ^{125}I-Aβ interactions with the BBB to irreversible ^{125}I-Aβ uptake into the BBB endothelium and brain parenchyma (Supplementary fig 1). The irreversible ^{125}I-Aβ kinetics were described by the influx clearance (K_i) assessed by the Patlak plots **(Fig. 2 C, Table II)**. The K_i for ^{25}I-Aβ42 (0.33 ± 0.07 µL/min) was found to be significantly (*p<0.05) higher than that of ^{125}I-Aβ40 (0.17 ± 0.03 µL/min).

Differences between ^{125}I-Aβ40 and ^{125}I-Aβ42 interactions with the BBB endothelium (Fig. 3, Table III). Upon IV bolus administration in WT mice, ^{125}I-Aβ concentrations were assessed in plasma and the brain (**Fig. 3 A)**. The brain concentrations were assayed by dynamic SPECT/CT imaging within 5 min following ^{125}I-Aβ administration and are assumed to be associated with the BBB endothelium. The compartmental model described in **Fig. 3 B** was simultaneously fitted to the plasma and BBB concentrations of ^{125}I-Aβ40 **(Fig. 3 C)** or ^{125}I-Aβ42 **(Fig. 3 D)**. The goodness-of-fit was established based on the Akaike criterion and the residual plots. The plasma PK parameter estimates **(Table III)** thus obtained for k_{12}, k_{21} and k_{10} showed statistically significant differences between ^{125}I-Aβ40 and ^{125}I-Aβ42. Additionally, the predicted volume of distribution (V) of ^{125}I-Aβ42 (16.47 ± 1.28 mL) was significantly greater than that of ^{125}I-Aβ40 (5.15 ± 0.37 mL). Moreover, influx (k_{13}) and efflux (k_{31}) rate constants between plasma and BBB, estimated from the dynamic SPECT/CT imaging data, were found to be significantly different between ^{125}I-Aβ40 and ^{125}I-Aβ42. Since, these peptides do not appreciably permeate the

JPET Fast Forward. Published on December 10, 2020 as DOI: 10.1124/jpet.120.000086
This article has not been copyedited and formatted. The final version may differ from this version.

BBB and reach the brain parenchyma in significant amounts within the first 5 min, k_{13} and k_{31} are expected to describe the interactions of ^{125}I-Aβ40 or ^{125}I-Aβ42 with their luminal receptors. The dissociation constant k_d, which is represented as the ratio of k_{31} to k_{13}, was also found to be substantially lower for ^{125}I-Aβ40 (107.5) than for ^{125}I-Aβ42 (355.5).

JPET Fast Forward. Published on December 10, 2020 as DOI: 10.1124/jpet.120.000086
This article has not been copyedited and formatted. The final version may differ from this version.

DISCUSSION

Cerebrovascular diseases such as small vessel disease, white matter hyper-intensities, and cerebral amyloid angiopathy were reported to contribute to approximately 40 % of all dementias, including Alzheimer's disease (AD). Although, underlying mechanisms are not completely understood, plasma Aβ appears to aggravate BBB dysfunction in cerebrovascular diseases (Goos *et al.,* 2012). It was claimed that the BBB dysfunction associated with these pathologies leads to a reduction in Aβ clearance from the brain and augment neuropathological changes, manifested as amyloid burden, tau tangles and neuronal loss (Kisler *et al.* , 2017). In the Rotterdam study, higher plasma Aβ levels were found to be associated with the greater incidence of cerebrovascular disease and cognitive decline in AD patients as well as in non-demented elderly participants (Hilal *et al.,* 2017). Plasma Aβ40 levels were shown to be strongly associated with diffuse small vessel disease (Gomis *et al.,* 2009), whereas higher plasma Aβ42 levels were found to be associated with white matter hyperintensity volume and greater incidence of infarcts on MRI (Gurol *et al.,* 2006; Toledo *et al.,* 2011). Additionally, chronic exposure of plasma Aβ40 and Aβ42 to the BBB endothelium was shown to produce vasoconstriction (Suhara *et al.,* 2003; Rice *et al.,* 2012) and vasomotor dysfunction (Park *et al.,* 2013); cerebral blood flow changes (Niwa *et al.,* 2000); and BBB leakage (Wan *et al.,* 2015). However, the toxicokinetics of plasma Aβ and the differential impact of Aβ40 and Aβ42 on the BBB dysfunction are not well understood.

The endocytosis of Aβ40 and Aβ42 at the BBB endothelium was reported to be mediated by the receptor for advanced glycation end products (RAGE) on the luminal side and low-density-lipoprotein receptor related protein 1 (LRP1) on the abluminal side. The Aβ40 demonstrated greater affinity to LRP1 and possibly to RAGE than Aβ42 (Deane *et al.,* 2004,

2009, 2012). Our studies in WT mice have shown that the efflux of ^{125}I-Aβ40 in the abluminal to luminal (A-L) direction is 1.5-fold greater than that of ^{125}I-Aβ42, but the influx of ^{125}I-Aβ42 in the luminal to abluminal (L-A) direction is about 4-fold greater than that of ^{125}I-Aβ40 (Swaminathan *et al.*, 2018). Hence, the differences between the transcytosis of Aβ40 and Aβ42 at the BBB endothelium could not be completely explained based on their affinities with the receptors. Our hypothesis is that the toxic exposure of Aβ peptides to the BBB is a consequence of changes in Aβ binding to the BBB endothelium, uptake, and their subsequent transcytosis.

We tested this hypothesis by investigating the uptake of Aβ40 and Aβ42 in the polarized hCMEC/D3 endothelial monolayers, which is a well-characterized human BBB model. (Weksler, 2005; Poller *et al.*, 2008). Although, polarized hCMEC/D3 monolayer model is known to have leakier tight junctions, its human origin would allow us to employ this model to investigate molecular mechanisms associated with cerebrovascular pathology in AD patients. Moreover, we employed hCMEC/D3 monolayers only to investigate the intra-endothelial accumulation of Aβ proteins, which gives us an estimate of BBB exposure to Aβ40 versus Aβ42. However, we did not investigate Aβ transcytosis in hCMEC/D3 monolayers, as it could be confounded by the leakier paracellular spaces in this model. Like previously reported by us (Kandimalla *et al.*, 2009) and others (Deane *et al.*, 2003), Aβ uptake by BBB endothelial cells is saturable and was significantly inhibited at 4 ºC. Based on this evidence, Aβ peptides are internalized by the BBB endothelium most likely by receptor mediated endocytosis. However, it was recently shown that Aβ-mediated decrease in claudin-5 and occludin expression may allow for size-selective paracellular movement of Aβ monomers, whereas the higher molecular weight Aβ oligomers may still encounter diffusional resistance and thus accumulate in the brain interstitial space (Keaney *et al.*, 2015). Although it is not clear if this is facilitated by the ability

JPET Fast Forward. Published on December 10, 2020 as DOI: 10.1124/jpet.120.000086
This article has not been copyedited and formatted. The final version may differ from this version.

of Aβ to transiently modulate actin cytoskeleton rearrangement in healthy brains, the study suggests the existence of such coordinated Aβ clearance processes at the BBB.

In our *in vitro* experiments, we observed that the unidirectional uptake of both Aβ40 and Aβ42 is polarized and is significantly greater in the L-A direction than in the A-L direction. We further observed that the rate of Aβ42 accumulation is higher than that of Aβ40 in L-A direction, whereas the rate of accumulation is similar for both Aβ40 and Aβ42 in the A-L direction.

To explore these *in vitro* findings, conventional methodologies using steady state measurements (Shibata *et al.*, 2000), microdialysis (Cirrito *et al.*, 2003), or capillary depletion techniques are inadequate, as they are not amenable to determining unidirectional rates of uptake in the L-A direction or vice versa. Hence, dynamic SPECT/CT imaging techniques were employed to determine the rates L-A transcytosis of Aβ40 versus Aβ42. Further, quantitative techniques were employed to temporally resolve initial interactions kinetics of ^{125}I-Aβ peptides with BBB endothelium from the transcytosis. Kinetics of ^{125}I-Aβ with the BBB endothelium during the first five minutes following intravenous administration was described by the Logan plot, which assumes that ^{125}I-Aβ on/off kinetics with the luminal receptors at these earliest time points are reversible. Moreover, the linearity of the Logan plot is lost at later time points (5-40 min), which is likely due to the entry of the tracer into the brain parenchyma- a kinetically irreversible compartment. The irreversibility ^{125}I-Aβ accumulation in the brain parenchyma at later time points satisfies the assumptions of the Patlak plot; hence, Patlak plots were employed to describe the transcytosis of ^{125}I-Aβ.

The slope of the Logan plot, which describes the distribution volume (V_T), was higher for ^{125}I-Aβ42 than for ^{125}I-Aβ40. Moreover, the influx clearance (K_i) into the irreversible brain compartment indicated by the slope of Patlak plot was higher for ^{125}I-Aβ42 than that of ^{125}I-

JPET Fast Forward. Published on December 10, 2020 as DOI: 10.1124/jpet.120.000086
This article has not been copyedited and formatted. The final version may differ from this version.

Aβ40. In fact, Logan slope (V_T) and Patlak slope (K_i) represent two complimentary parameters of L-A transcytosis. Higher V_T value of ^{125}I-Aβ42 suggests robust interaction of Aβ42 with the BBB endothelium compared to ^{125}I-Aβ40. Similarly, higher K_i of ^{125}I-Aβ42 compared to ^{125}I-Aβ40 is indicative of greater brain influx of ^{125}I-Aβ42 compared to ^{125}I-Aβ40. These global trends were further resolved into individual rates by simultaneously fitting plasma and brain data to a compartmental model.

Distinct plasma-to-BBB transfer rate constants for ^{125}I-Aβ40 and ^{125}I-Aβ42 were predicted by the compartmental model. The influx rate constant (k_{13}) of ^{125}I-Aβ42 was higher than that of ^{125}I-Aβ40. Moreover, the product of k_{13} and V, which refers to influx clearance CL_i from plasma-to-BBB, was predicted to be higher for ^{125}I-Aβ42 compared to that of ^{125}I-Aβ40. This is in line with the Patlak plot predictions of higher K_i for ^{125}I-Aβ42 than that of ^{125}I-Aβ40. Moreover, the ratio of k_{31} to k_{13} (k_{31}/k_{13}), an estimate of the dissociation constant (k_d), is higher for ^{125}I-Aβ42 compared to ^{125}I-Aβ40. These results indicate that despite the higher affinity of ^{125}I-Aβ40 to the luminal BBB receptors compared to that of ^{125}I-Aβ42, the L-A transcytosis of ^{125}I-Aβ40 was lower. It is not uncommon for macromolecules to demonstrate greater affinity for the receptors (Thomas, 2000) but show ineffective transcytosis; hence, reduction of receptor affinity is often pursued as a strategy to improve the transcytosis of such molecules (Bien-Ly *et al.*, 2014). While it is possible that the lower ability of ^{125}I-Aβ40 to transcytose across the BBB endothelium is due to its greater receptor affinity, it may also result from the ability of vasculotropic Aβ40 to inhibit its own exocytosis (Agyare *et al.*, 2013), most likely by interfering with the SNARE assemblies (Sharda *et al.*, 2020). It would be interesting to evaluate how these distinct profiles impact the clearance of abluminal Aβ and Aβ plaques in the brain. These aspects are currently being investigated in our laboratory.

JPET Fast Forward. Published on December 10, 2020 as DOI: 10.1124/jpet.120.000086
This article has not been copyedited and formatted. The final version may differ from this version.

Although our current study highlights the differences in the kinetics of luminal Aβ40 and Aβ42, it does not predict any molecular mediators that could potentially lead to these differences. In addition, we did not investigate the impact of plasma protein [albumin, ApoE, ApoJ, soluble LRP (sLRP), soluble RAGE (sRAGE), etc.] binding on the systemic clearance and BBB uptake of Aβ40 versus Aβ42. Another methodological constraint that warrants careful interpretation of the kinetic data is the use of supraphysiological ^{125}I-Aβ doses in SPECT/CT imaging studies to enhance the brain signal. While 10-11 μg of ^{125}I-Aβ was administered as an IV bolus injection in SPECT/CT studies, 2-2.2 μg ^{125}I-Aβ was injected in the plasma PK studies. Based on the volumes of distribution of Aβ40 and Aβ42, these doses are expected to generate plasma concentrations of 2 μg/ml for Aβ40 and 0.6 μg/ml for Aβ42 in SPECT studies. Similarly, in PK studies Aβ40 and Aβ42 plasma concentrations are expected to be around 0.4 and 0.12 μg/ml, respectively. Despite substantial differences in plasma Aβ concentrations, differences between Aβ40 and Aβ42 uptake rates at the BBB were consistent, as observed in our earlier studies (Swaminathan et al., 2018). These results suggest that the relative differences in Aβ40 and Aβ42 uptake at the BBB remain consistent across a wide range of plasma concentrations, including at the plasma Aβ levels observed in Alzheimer's patients and transgenic mice.

In summary, Aβ40 and Aβ42 exhibit differential trafficking kinetics at the BBB endothelium under normal physiological conditions. While luminal Aβ40 demonstrated greater affinity to the BBB endothelium compared to Aβ42, rate of Aβ42 uptake from plasma and its subsequent transcytosis into the brain is significantly higher than that of Aβ40. During Alzheimer's progression and in cerebrovascular disease, the physiological machinery that orchestrate Aβ trafficking at the BBB could be disrupted and result in anomalous Aβ exposure to the BBB endothelium. This in turn could unleash downstream toxic effects on the cerebral microvasculature and aggravate neurocognitive changes.

Acknowledgements:

Authors would like to acknowledge Dr. Rajesh S. Omtri posthumously for his contribution to the project in terms of experimentation and valuable discussions. The authors would also like to acknowledge the technical help from Mrs. Teresa Decklever in conducting SPECT/CT studies.

Author contribution statement:

Participated in research design: Sharda and Kandimalla

Conducted experiments: Sharda, Ahlschwede and Curran

Contributed new reagents or analytical tools: Lowe and Kandimalla

Performed data analysis: Sharda, Ahlschwede and Kandimalla

Wrote or contributed to the writing of the manuscript: Sharda and Kandimalla. The final manuscript was reviewed by all the authors.

Conflict of Interest:

Dr. Lowe consults for Bayer Schering Pharma, Piramal Life Sciences and Merck Research and receives research support from GE Healthcare, Siemens Molecular Imaging, AVID Radiopharmaceuticals and the NIH (NIA, NCI).

JPET Fast Forward. Published on December 10, 2020 as DOI: 10.1124/jpet.120.000086
This article has not been copyedited and formatted. The final version may differ from this version.

References

Agyare EK, Leonard SR, Curran GL, Yu CC, Lowe VJ, Paravastu AK, Poduslo JF, and Kandimalla KK (2013) Traffic jam at the blood-brain barrier promotes greater accumulation of Alzheimer's disease amyloid-β proteins in the cerebral vasculature. *Mol Pharm* **10**:1557–1565.

Ascolani A, Balestrieri E, Minutolo A, Mosti S, Spalletta G, Bramanti P, Mastino A, Caltagirone C, and Macchi B (2012) Dysregulated NF-κB Pathway in Peripheral Mononuclear Cells of Alzheimer's Disease Patients. *Curr Alzheimer Res* **9**:128–137.

Bell RD, Sagare AP, Friedman AE, Bedi GS, Holtzman DM, Deane R, and Zlokovic B V (2007) Transport pathways for clearance of human Alzheimer's amyloid beta-peptide and apolipoproteins E and J in the mouse central nervous system. *J Cereb Blood Flow Metab* **27**:909–18.

Bien-Ly N, Yu YJ, Bumbaca D, Elstrott J, Boswell CA, Zhang Y, Luk W, Lu Y, Dennis MS, Weimer RM, Chung I, and Watts RJ (2014) Transferrin receptor (TfR) trafficking determines brain uptake of TfR antibody affinity variants. *J Exp Med* **211**:233–244.

Bowman GL, and Quinn JF (2008) Alzheimer's disease and the Blood-Brain Barrier: Past, Present and Future. *Aging health* **4**:47–55, NIH Public Access.

Cirrito JR, May PC, O'Dell MA, Taylor JW, Parsadanian M, Cramer K, Cramer JW, Audia JE, Nissen JS, Bales KR, Paul SM, DeMattos RB, and Holtzman DM (2003) In Vivo Assessment of Brain Interstitial Fluid with Microdialysis reveals Plaque-Associated Changes in Amyloid-β Metabolism and Half-Life. *Neuroscience* **23**:8844–8853, Society for Neuroscience.

Cleary JP, Walsh DM, Hofmeister JJ, Shankar GM, Kuskowski MA, Selkoe DJ, and Ashe KH (2005) Natural oligomers of the amyloid-beta protein specifically disrupt cognitive function. *Nat Neurosci* **8**:79–84.

Deane R, Bell RD, Sagare A, and Zlokovic B V (2009) Clearance of amyloid-beta peptide

across the blood-brain barrier: implication for therapies in Alzheimer's disease. *CNS Neurol Disord Drug Targets* **8**:16–30.

Deane R, Du Yan S, Submamaryan RK, LaRue B, Jovanovic S, Hogg E, Welch D, Manness L, Lin C, Yu J, Zhu H, Ghiso J, Frangione B, Stern A, Schmidt AM, Armstrong DL, Arnold B, Liliensiek B, Nawroth P, Hofman F, Kindy M, Stern D, and Zlokovic B (2003) RAGE mediates amyloid-beta peptide transport across the blood-brain barrier and accumulation in brain. *Nat Med* **9**:907–913.

Deane R, Wu Z, Sagare A, Davis J, Du Yan S, Hamm K, Xu F, Parisi M, LaRue B, Hu HW, Spijkers P, Guo H, Song X, Lenting PJ, Van Nostrand WE, and Zlokovic B V. (2004) LRP/amyloid beta-peptide interaction mediates differential brain efflux of Abeta isoforms. *Neuron* **43**:333–44.

Deane RJRJ, Singh I, Sagare AP, Bell RD, Ross NT, LaRue B, Love R, Perry S, Paquette N, Deane RJRJ, Thiyagarajan M, Zarcone T, Fritz G, Friedman AE, Miller BL, and Zlokovic B V (2012) A multimodal RAGE-specific inhibitor reduces amyloid beta-mediated brain disorder in a mouse model of Alzheimer disease. *J Clin Invest* **122**:1377–1392.

DeMattos RB, Bales KR, Cummins DJ, Dodart JC, Paul SM, and Holtzman DM (2001) Peripheral anti-Aβ antibody alters CNS and plasma Aβ clearance and decreases brain Aβ burden in a mouse model of Alzheimer's disease. *Proc Natl Acad Sci U S A* **98**:8850–8855.

Eisele YS, Fritschi SK, Hamaguchi T, Obermüller U, Füger P, Skodras A, Schäfer C, Odenthal J, Heikenwalder M, Staufenbiel M, and Jucker M (2014) Multiple Factors Contribute to the Peripheral Induction of Cerebral β-Amyloidosis. *J Neurosci* **34**:10264–73.

Erickson M a, and Banks W a (2013) Blood-brain barrier dysfunction as a cause and consequence of Alzheimer's disease. *J Cereb Blood Flow Metab* **33**:1500–13.

Fandos N, Pérez-Grijalba V, Pesini P, Olmos S, Bossa M, Villemagne VL, Doecke J, Fowler C, Masters CL, Sarasa M, and AIBL Research Group (2017) Plasma amyloid β 42/40 ratios as biomarkers for amyloid β cerebral deposition in cognitively normal individuals.

Alzheimer's Dement Diagnosis, Assess Dis Monit **8**:179–187.

Gomis M, Sobrino T, Ois A, Millán M, Rodríguez-Campello A, de la Ossa NP, Rodríguez-González R, Jiménez-Conde J, Cuadrado-Godia E, Roquer J, and Dávalos A (2009) Plasma β-Amyloid 1-40 Is Associated With the Diffuse Small Vessel Disease Subtype. *Stroke* **40**:3197–3201.

Goos JD, Teunissen CE, Veerhuis R, Verwey NA, Barkhof F, Blankenstein MA, Scheltens P, and van der Flier WM (2012) Microbleeds relate to altered amyloid-beta metabolism in Alzheimer's disease. *Neurobiol Aging* **33**.

Govindpani K, McNamara LG, Smith NR, Vinnakota C, Waldvogel HJ, Faull RL, and Kwakowsky A (2019) Vascular Dysfunction in Alzheimer's Disease: A Prelude to the Pathological Process or a Consequence of It? *J Clin Med* **8**:651.

Gurol ME, Irizarry MC, Smith EE, Raju S, Diaz-Arrastia R, Bottiglieri T, Rosand J, Growdon JH, and Greenberg SM (2006) Plasma -amyloid and white matter lesions in AD, MCI, and cerebral amyloid angiopathy. *Neurology* **66**:23–29.

Hilal S, Akoudad S, van Duijn CM, Niessen WJ, Verbeek MM, Vanderstichele H, Stoops E, Ikram MA, and Vernooij MW (2017) Plasma Amyloid-β Levels, Cerebral Small Vessel Disease, and Cognition: The Rotterdam Study. *J Alzheimer's Dis* **60**:977–987.

Hu X, Li X, Zhao M, Gottesdiener A, Luo W, and Paul S (2014) Tau pathogenesis is promoted by Aβ1-42 but not Aβ1-40. *Mol Neurodegener* **9**:52.

Kandimalla KK, Curran GL, Holasek SS, Gilles EJ, Wengenack TM, and Poduslo JF (2005) Pharmacokinetic analysis of the blood-brain barrier transport of 125I-amyloid beta protein 40 in wild-type and Alzheimer's disease transgenic mice (APP,PS1) and its implications for amyloid plaque formation. *J Pharmacol Exp Ther* **313**:1370–1378.

Kandimalla KK, Scott OG, Fulzele S, Davidson MW, and Poduslo JF (2009) Mechanism of neuronal versus endothelial cell uptake of Alzheimer's disease amyloid beta protein. *PLoS One* **4**:e4627.

Keaney J, Walsh DM, O'Malley T, Hudson N, Crosbie DE, Loftus T, Sheehan F, McDaid J, Humphries MM, Callanan JJ, Brett FM, Farrell MA, Humphries P, and Campbell M (2015) Autoregulated paracellular clearance of amyloid-β across the blood-brain barrier. *Sci Adv* **1**:e1500472, American Association for the Advancement of Science.

Khan AI, Liu J, and Dutta P (2018) Iron transport kinetics through blood-brain barrier endothelial cells. *Biochim Biophys Acta - Gen Subj* **1862**:1168–1179, Elsevier B.V.

Kisler K, Nelson AR, Montagne A, and Zlokovic B V. (2017) Cerebral blood flow regulation and neurovascular dysfunction in Alzheimer disease. *Nat Rev Neurosci* **18**:419–434.

Klein W., Stine W., and Teplow D. (2004) Small assemblies of unmodified amyloid β-protein are the proximate neurotoxin in Alzheimer's disease. *Neurobiol Aging* **25**:569–580.

Koizumi K, Wang G, and Park L (2016) Endothelial Dysfunction and Amyloid-β-Induced Neurovascular Alterations. *Cell Mol Neurobiol* **36**:155–65, NIH Public Access.

Lacor PN, Buniel MC, Furlow PW, Clemente AS, Velasco PT, Wood M, Viola KL, and Klein WL (2007) Abeta oligomer-induced aberrations in synapse composition, shape, and density provide a molecular basis for loss of connectivity in Alzheimer's disease. *J Neurosci* **27**:796–807.

Li G, Yuan W, and Fu BM (2010) A model for the blood-brain barrier permeability to water and small solutes. *J Biomech* **43**:2133–2140, Elsevier.

Logan J, Fowler JS, Volkow ND, Wolf AP, Dewey SL, Schlyer DJ, MacGregor RR, Hitzemann R, Bendriem B, and Gatley SJ (1990) Graphical analysis of reversible radioligand binding from time-activity measurements applied to [N-11C-methyl]-(-)-cocaine PET studies in human subjects. *J Cereb Blood Flow Metab* **10**:740–7.

Marchi N, Cavaglia M, Fazio V, Bhudia S, Hallene K, and Janigro D (2004) Peripheral markers of blood-brain barrier damage. *Clin Chim Acta* **342**:1–12.

Marques MA, Kulstad JJ, Savard CE, Green PS, Lee SP, Craft S, Watson GS, and Cook DG (2009) Peripheral amyloid-beta levels regulate amyloid-beta clearance from the central

nervous system. *J Alzheimers Dis* **16**:325–9.

Niwa K, Carlson GA, and Iadecola C (2000) Exogenous Aβ1–40 Reproduces Cerebrovascular Alterations Resulting from Amyloid Precursor Protein Overexpression in Mice. *J Cereb Blood Flow Metab* **20**:1659–1668, SAGE PublicationsSage UK: London, England.

Omtri RS, Davidson MW, Arumugam B, Poduslo JF, and Kandimalla KK (2012) Differences in the Cellular Uptake and Intracellular Itineraries of Amyloid Beta Proteins 40 and 42: Ramifications for the Alzheimer's Drug Discovery. *Mol Pharm* **9**:1887–1897.

Park L, Zhou P, Koizumi K, El Jamal S, Previti M Lou, Van Nostrand WE, Carlson G, and Iadecola C (2013) Brain and circulating levels of Aβ1-40 differentially contribute to vasomotor dysfunction in the mouse brain. *Stroke* **44**:198–204, Lippincott Williams & WilkinsHagerstown, MD.

Patlak CS, Blasberg RG, and Fenstermacher JD (1983) Graphical evaluation of blood-to-brain transfer constants from multiple-time uptake data. *J Cereb Blood Flow Metab* **3**:1–7.

Poduslo JF, Curran GL, Haggard JJ, Biere a L, and Selkoe DJ (1997) Permeability and residual plasma volume of human, Dutch variant, and rat amyloid beta-protein 1-40 at the blood-brain barrier. *Neurobiol Dis* **4**:27–34.

Poljak A, and Sachdev PS (2017) Plasma amyloid beta peptides: an Alzheimer's conundrum or a more accessible Alzheimer's biomarker? *Expert Rev Neurother* **17**:3–5, Taylor & Francis.

Poller B, Gutmann H, Krähenbühl S, Weksler B, Romero I, Couraud PO, Tuffin G, Drewe J, and Huwyler J (2008) The human brain endothelial cell line hCMEC/D3 as a human blood-brain barrier model for drug transport studies. *J Neurochem* **107**:1358–1368.

Rice HC, Townsend M, Bai J, Suth S, Cavanaugh W, Selkoe DJ, and Young-Pearse TL (2012) Pancortins interact with amyloid precursor protein and modulate cortical cell migration. *Development* **139**:3986–96.

Ryan SD, Whitehead SN, Swayne LA, Moffat TC, Hou W, Ethier M, Bourgeois AJG, Rashidian J, Blanchard AP, Fraser PE, Park DS, Figeys D, and Bennett SAL (2009) Amyloid-beta42

signals tau hyperphosphorylation and compromises neuronal viability by disrupting alkylacylglycerophosphocholine metabolism. *Proc Natl Acad Sci U S A* **106**:20936–41.

Sharda N, Pengo T, Wang Z, and Kandimalla K (2020) Amyloid-β Peptides Disrupt Interactions Between VAMP-2 and SNAP-25 in Neuronal Cells as Determined by FRET/FLIM. *J Alzheimer's Dis* **77**:1–13, IOS Press.

Shibata M, Yamada S, Ram Kumar S, Calero M, Bading J, Frangione B, Holtzman DM, Miller C a., Strickland DK, Ghiso J, and Zlokovic B V. (2000) Clearance of Alzheimer's amyloid-β1-40 peptide from brain by LDL receptor-related protein-1 at the blood-brain barrier. *J Clin Invest* **106**:1489–1499.

Suhara T, Magrané J, Rosen K, Christensen R, Kim HS, Zheng B, McPhie DL, Walsh K, and Querfurth H (2003) Aβ42 generation is toxic to endothelial cells and inhibits eNOS function through an Akt/GSK-3β signaling-dependent mechanism. *Neurobiol Aging* **24**:437–451, Neurobiol Aging.

Swaminathan SK, Ahlschwede KM, Sarma V, Curran GL, Omtri RS, Decklever T, Lowe VJ, Poduslo JF, and Kandimalla KK (2018) Insulin differentially affects the distribution kinetics of amyloid beta 40 and 42 in plasma and brain. *J Cereb Blood Flow Metab* **38**:904–918.

Thomas GD (2000) Effect of Dose, Molecular Size, and Binding Affinity on Uptake of Antibodies, in *Drug Targeting* pp 115–132, Humana Press, New Jersey.

Toledo JB, Shaw LM, and Trojanowski JQ (2013) Plasma amyloid beta measurements - a desired but elusive Alzheimer's disease biomarker. *Alzheimers Res Ther* **5**:8.

Toledo JB, Vanderstichele H, Figurski M, Aisen PS, Petersen RC, Weiner MW, Jack CR, Jagust W, Decarli C, Toga AW, Toledo E, Xie SX, Lee VMY, Trojanowski JQ, and Shaw LM (2011) Factors affecting Aβ plasma levels and their utility as biomarkers in ADNI. *Acta Neuropathol* **122**:401–413, Springer.

van Oijen M, Hofman A, Soares HD, Koudstaal PJ, and Breteler MM (2006) Plasma Aβ1–40 and Aβ1–42 and the risk of dementia: a prospective case-cohort study. *Lancet Neurol*

5:655–660.

Wan W, Cao L, Liu L, Zhang C, Kalionis B, Tai X, Li Y, and Xia S (2015) Aβ1-42 oligomer-induced leakage in an in vitro blood-brain barrier model is associated with up-regulation of RAGE and metalloproteinases, and down-regulation of tight junction scaffold proteins. *J Neurochem* **134**:382–393, Blackwell Publishing Ltd.

Weksler BB (2005) Blood-brain barrier-specific properties of a human adult brain endothelial cell line. *FASEB J* **26**:1–26.

Younkin SG (1998) The role of A beta 42 in Alzheimer's disease. *J Physiol Paris* **92**:289–92.

Zlokovic B V (2010) Neurodegeneration and the neurovascular unit. *Nat Med* **16**:1370–1371, Nature Publishing Group.

Zlokovic B V (2011) Neurovascular pathways to neurodegeneration in Alzheimer's disease and other disorders. *Nat Rev Neurosci* **12**:723–38, NIH Public Access.

JPET Fast Forward. Published on December 10, 2020 as DOI: 10.1124/jpet.120.000086
This article has not been copyedited and formatted. The final version may differ from this version.

Footnotes

This work was supported by the Minnesota Partnership Grant # 15.31

This work is part of the Ph.D. dissertation submitted to the University of Minnesota

Sharda, Nidhi. (2016). Trafficking of Amyloid beta protein at the Blood Brain Barrier: Novel Insights in Alzheimer's Disease Pathogenesis. Retrieved from the University of Minnesota Digital Conservancy, http://hdl.handle.net/11299/194548.

Reprint requests:

Karunya K. Kandimalla

Department of Pharmaceutics and the Brain Barriers Research Center, College of Pharmacy, University of Minnesota, Minneapolis, MN 55455, USA

Email: kkandima@umn.edu

JPET Fast Forward. Published on December 10, 2020 as DOI: 10.1124/jpet.120.000086
This article has not been copyedited and formatted. The final version may differ from this version.

Figure Legends:

Figure 1. Distinct uptake kinetics of F-Aβ40 and F-Aβ42 in hCMEC/D3 cells. **A.** Experimental design describing **B.** total (37 ℃, filled) and non-specific (4 ℃, open) uptake of F-Aβ40 (circle) or F-Aβ42 (square) in hCMEC/D3 cells incubated with increasing concentrations of F-Aβ peptides. Data is presented as geometric mean ± geometric S.D. **C.** Experimental design describing the accumulation of F-Aβ40 (filled square) and F-Aβ42 (open square) in polarized hCMEC/D3 cell monolayers over time in **D.** luminal-abluminal (L-A) and **E.** abluminal-luminal (A-L) direction. Linear regression slopes (Table I) were estimated and compared using Student's t-test (***$p < 0.001$).

Figure 2. Kinetics of BBB interactions (Logan plot) and brain uptake (Patlak plot) of ^{125}I-Aβ40 and ^{125}I-Aβ42 in WT mice. **A.** Experimental design; **B.** Distribution volumes (V_T) of ^{125}I-Aβ40 (filled circle) and ^{125}I-Aβ42 (filled square) determined by the Logan plot; and **C.** Brain influx clearance rates (K_i) of ^{125}I-Aβ40 (open circle) and ^{125}I-Aβ42 (filled square) determined by the Patlak plot. Corresponding slopes (Table II) are presented as the mean ± standard error. The statistical significance between ^{125}I-Aβ40 and ^{125}I-Aβ42 was assessed by Student's t-test (*$p<0.05$ and *** $p<0.001$).

Figure 3. Distinct plasma-BBB uptake kinetics of ^{125}I-Aβ40 and ^{125}I-Aβ42 in WT mice. **A.** Experimental design; **B.** Three compartment pharmacokinetic model describing plasma kinetics and interactions with the BBB endothelium of **C.** ^{125}I-Aβ40 and **D.** ^{125}I-Aβ42. Plasma: filled circles represent observed values and dashed lines correspond to the predicted data. BBB: open circles represent observed values and solid lines show predicted data. Corresponding model

JPET Fast Forward. Published on December 10, 2020 as DOI: 10.1124/jpet.120.000086
This article has not been copyedited and formatted. The final version may differ from this version.

predicted parameters of ^{125}I-Aβ40 and ^{125}I-Aβ42 are presented (Table III) as mean (per cent coefficient of variance). Significance determined by Student's t-test (*$p < 0.05$, **$p<0.01$, ***$p<0.001$)

JPET Fast Forward. Published on December 10, 2020 as DOI: 10.1124/jpet.120.000086
This article has not been copyedited and formatted. The final version may differ from this version.

Tables:

Table I. Kinetics of F-Aβ40 and F-Aβ42 uptake by polarized hCMEC/D3 cell monolayers

Slope parameter (IFU/min)	F-Aβ40	F-Aβ42	Significance
Luminal-Abluminal (L-A)	0.55 ± 0.04	1.79 ± 0.12	***
Abluminal-Luminal (A-L)	0.11 ± 0.003	0.11 ± 0.01	N.S.

Data presented as Slope ± SD. Significance determined by Student's t-test (***$p<0.001$) IFU stands for intracellular fluorescence units.

JPET Fast Forward. Published on December 10, 2020 as DOI: 10.1124/jpet.120.000086
This article has not been copyedited and formatted. The final version may differ from this version.

Table II. Graphical model predicted slope parameters of ^{125}I-Aβ40 and ^{125}I-Aβ42

Graphical model	Slope parameter (units)	F-Aβ40	F-Aβ42	Significance
Logan Plot	Distribution volume, V_T (μL)	39.7 ± 0.07	55.8 ± 1.2	***
Patlak Plot	Influx clearance, K_i (μL/min)	0.17 ± 0.03	0.33 ± 0.07	*

Data presented as Slope ± SE. Significance determined by Student's t-test (*p < 0.05, ***p<0.001)

JPET Fast Forward. Published on December 10, 2020 as DOI: 10.1124/jpet.120.000086
This article has not been copyedited and formatted. The final version may differ from this version.

Table III. Pharmacokinetic model predicted parameters of ^{125}I-Aβ40 and ^{125}I-Aβ42

Parameter	Units	^{125}I-Aβ40	^{125}I-Aβ42	Significance
$\boldsymbol{k_{12}}$	min^{-1}	0.59 (15)	1.32 (29)	*
$\boldsymbol{k_{21}}$	min^{-1}	0.50 (6)	1.37 (10)	***
$\boldsymbol{k_{10}}$	min^{-1}	0.44 (13)	0.19 (10)	**
$\boldsymbol{k_{13}}$	min^{-1}	0.004 (15)	0.009 (12)	***
$\boldsymbol{k_{31}}$	min^{-1}	0.43 (13)	3.2 (11)	***
$\boldsymbol{k_d}$ **or** $\boldsymbol{k_{31}/k_{13}}$	$unitless$	107.5	355.5	-
$\boldsymbol{V}$	mL	5.15 (7)	16.47 (8)	***
$\boldsymbol{CL_i}$ **or** $\boldsymbol{k_{13}} \times \boldsymbol{V}$	mL/min	0.02	0.15	-

Data presented as mean (coefficient of variance expressed as per cent). Significance determined by Student's t-test (*p < 0.05, **p<0.01, ***p<0.001).

k_d and CL_i calculated as described using mean parameter estimates. No significance was determined.

JPET Fast Forward. Published on December 10, 2020 as DOI: 10.1124/jpet.120.000086
This article has not been copyedited and formatted. The final version may differ from this version.

Figure 1.

JPET Fast Forward. Published on December 10, 2020 as DOI: 10.1124/jpet.120.000086
This article has not been copyedited and formatted. The final version may differ from this version.

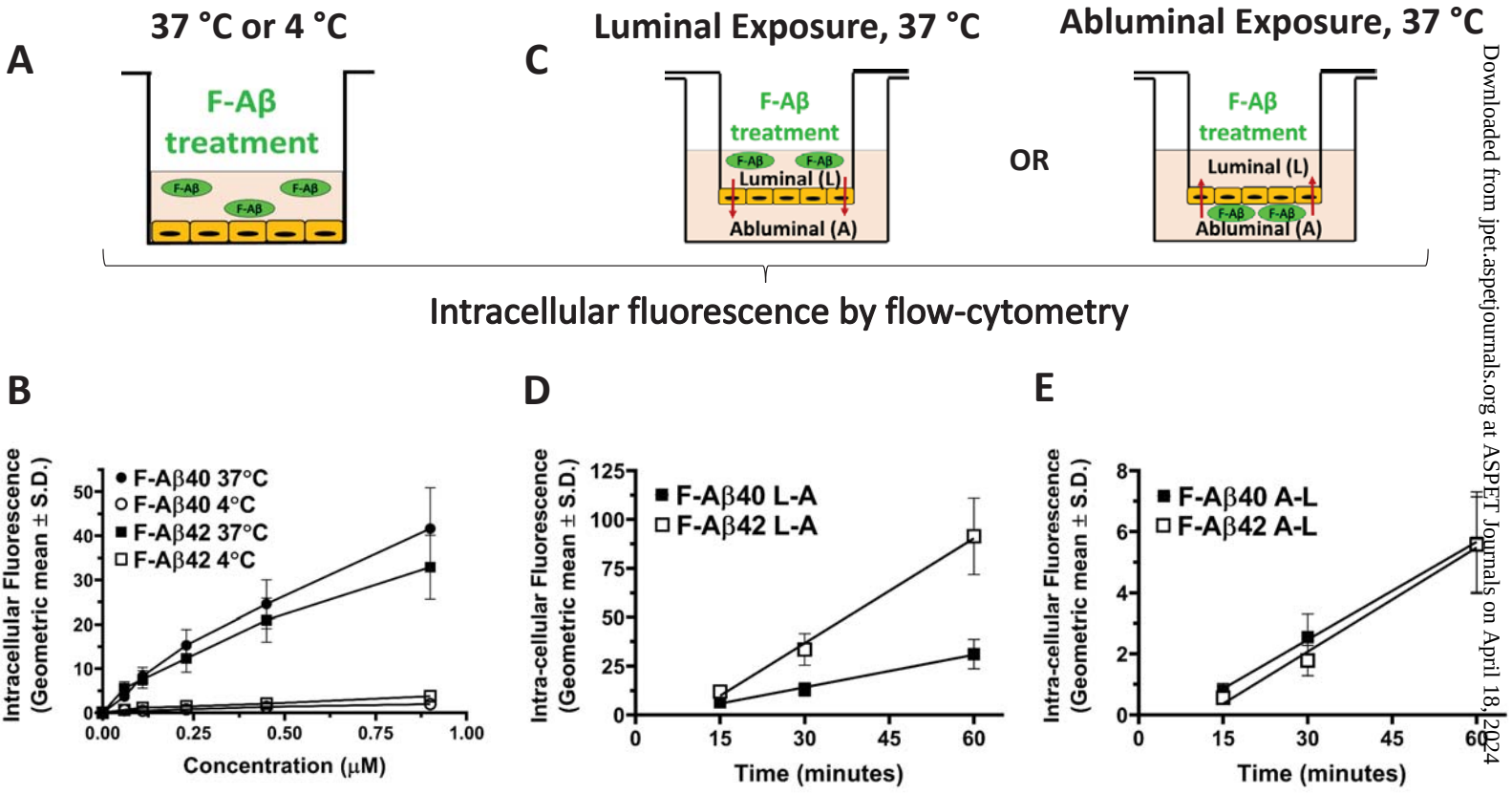

JPET Fast Forward. Published on December 10, 2020 as DOI: 10.1124/jpet.120.000086
This article has not been copyedited and formatted. The final version may differ from this version.

Figure 2.

JPET Fast Forward. Published on December 10, 2020 as DOI: 10.1124/jpet.120.000086
This article has not been copyedited and formatted. The final version may differ from this version.

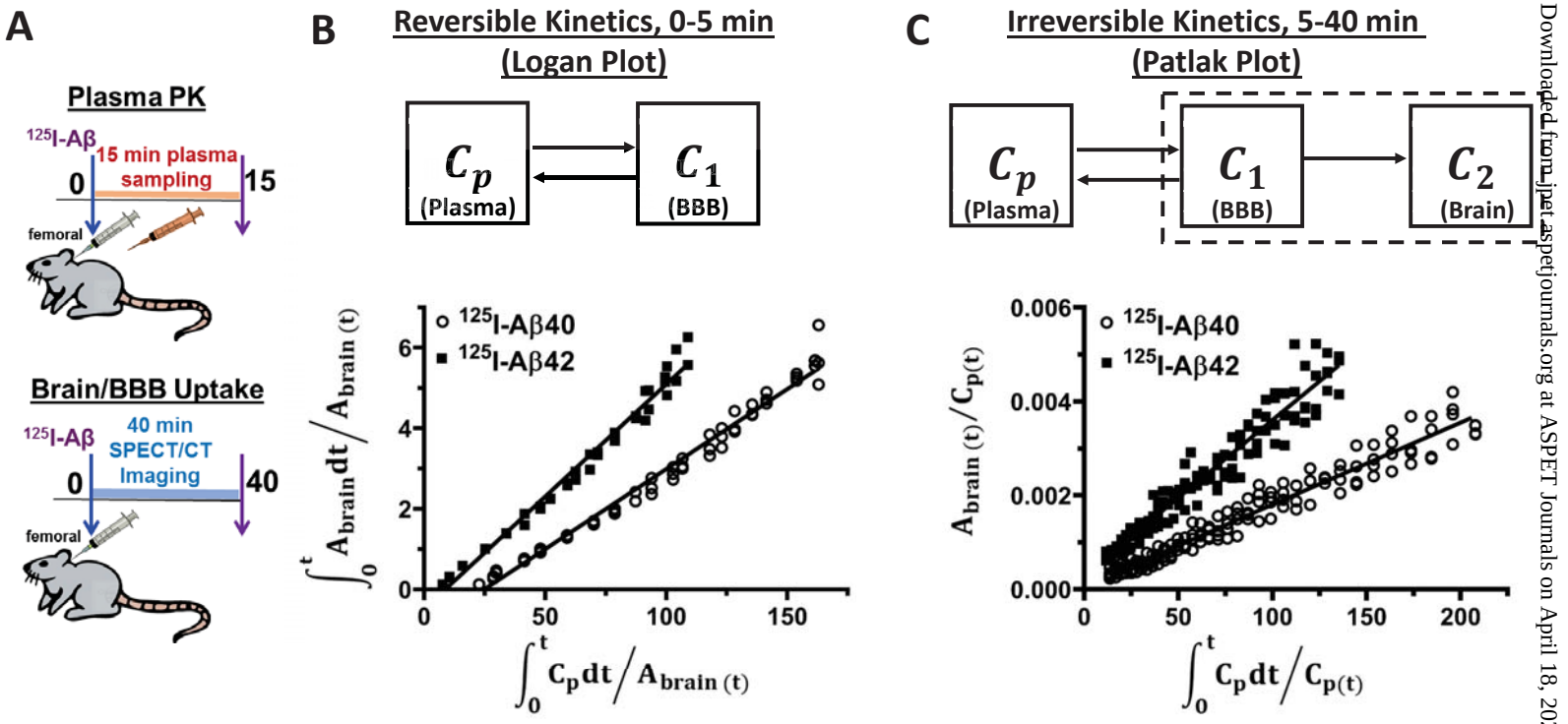

JPET Fast Forward. Published on December 10, 2020 as DOI: 10.1124/jpet.120.000086
This article has not been copyedited and formatted. The final version may differ from this version.

Figure 3.

JPET Fast Forward. Published on December 10, 2020 as DOI: 10.1124/jpet.120.000086
This article has not been copyedited and formatted. The final version may differ from this version.

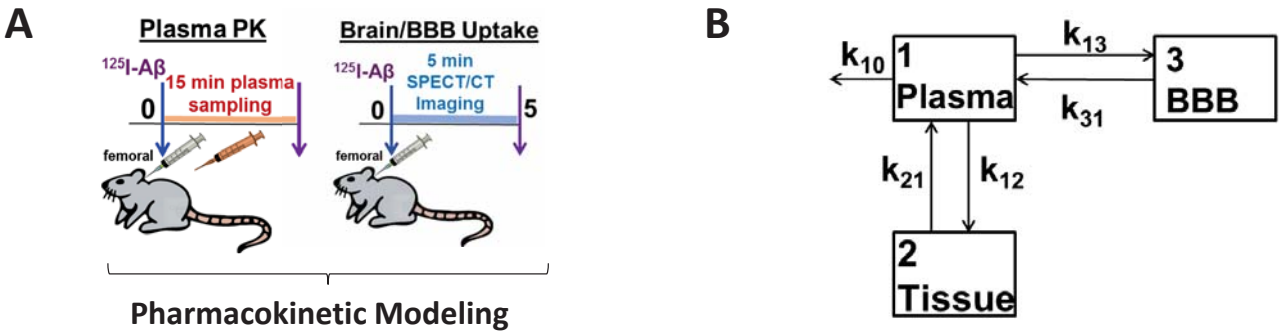

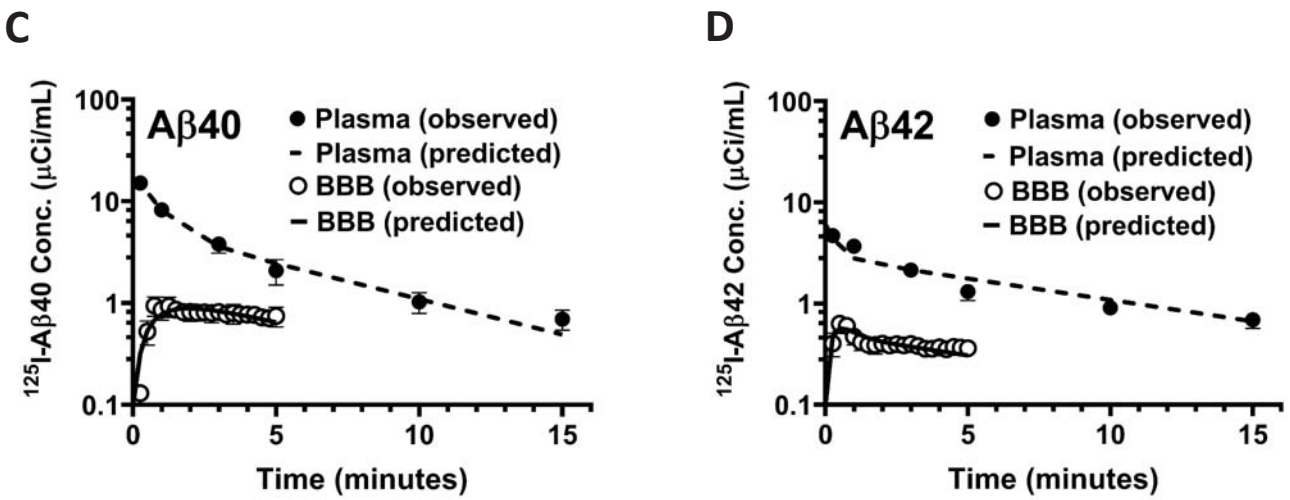

Supplementary Section

Article title: ***Distinct uptake kinetics of Alzheimer's disease amyloid beta (Aβ) 40 and 42 at the blood-brain barrier endothelium***

Authors: Nidhi Sharda, Kristen M. Ahlschwede, Geoffry L. Curran, Val J. Lowe and Karunya K. Kandimalla

Journal title: Journal of Pharmacology and Experimental Therapeutics

Manuscript number: JPET-AR-2020-000086

Supplementary Figure 1.

Article title: *Distinct uptake kinetics of Alzheimer's disease amyloid beta (Aβ) 40 and 42 at the blood-brain barrier endothelium*
Authors: Nidhi Sharda, Kristen M. Ahlschwede, Geoffry L. Curran, Val J. Lowe and Karunya K. Kandimalla
Journal title: Journal of Pharmacology and Experimental Therapeutics. Manuscript number: JPET-AR-2020-000086

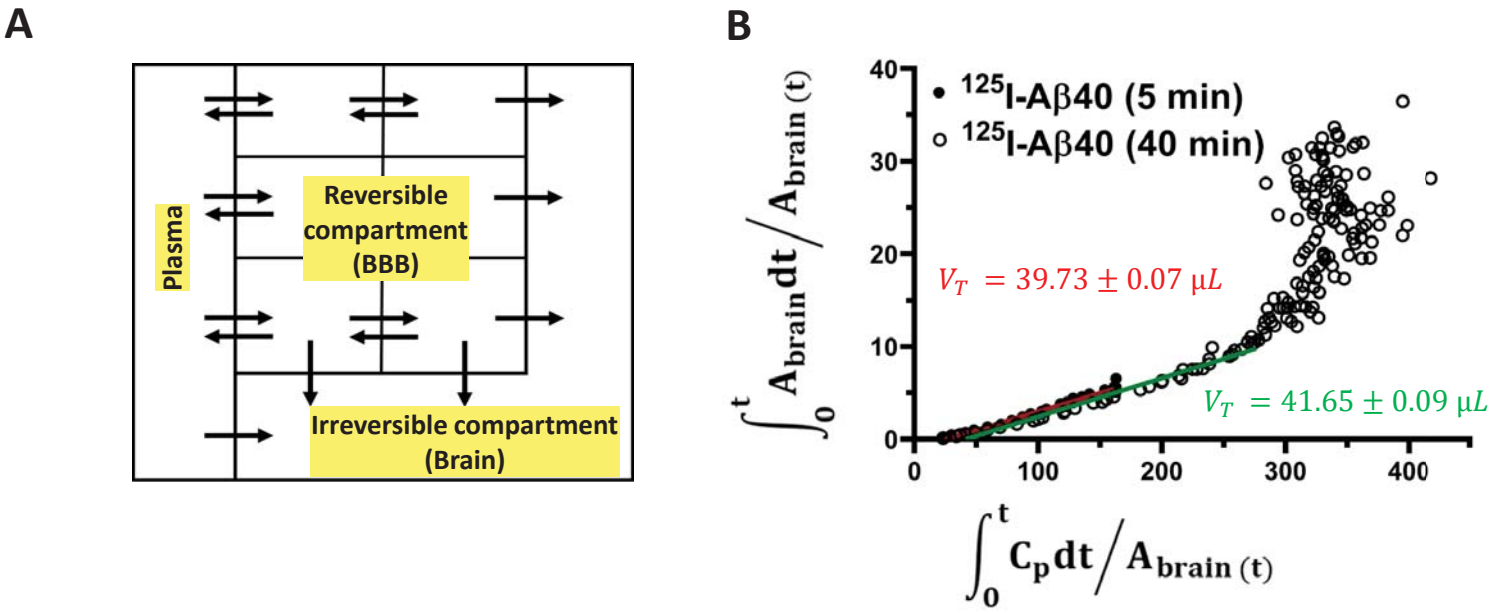

Supplementary figure 1 A Representative blood-brain exchange model structure comprising of reversible region of *n* compartments that freely exchanges with plasma, described by Logan plot; irreversible (brain) region where solute enters irreversibly is described by Patlak plot. **B** Linear slopes of Logan plot describes the reversible uptake of ^{125}I-Aβ40 into the BBB endothelium for initial 5 minutes. Logan plots of ^{125}I-Aβ40 at 0-5 minutes (closed circle) and from 0 to 40 minutes (open circles) were obtained. Volume of distribution (V_T) obtained from the slopes of linear regression line predicted by the model for ^{125}I-Aβ40 at 0-5 (red) and 0-40 (green) minutes (estimate ± standard error) overlay initially but deviates significantly at later time points, most likely due to the violation of reversibility assumption.